Check for updates

Li$_{4x/3}$Co$_{2-2x}$Ti$_{1+2x/3}$O$_4$ spinel solid solutions: order and disorder phase transition, cations distribution and adjustable microwave dielectric properties

Xianghu Tan,[a] Huanfu Zhou, [ID] *[a] Yuxin Tang, [ID] [b] Di Zhou,[c] Pushkar Kanhere,[b] Qiuling Tay[b] and Xiuli Chen[a]

A series of spinel solid solutions Li$_{4x/3}$Co$_{2-2x}$Ti$_{1+2x/3}$O$_4$ (LCT, $0.2 \leq x \leq 0.8$) were synthesized and their structures and microwave dielectric properties were characterized in detail. The distribution of cations at A and B sites in the lattice has been analyzed by using Rietveld refinement. The microstructure and dielectric properties were studied by scanning electron microscope and microwave network analyzer. The solid solutions undergo a discontinuous B-site, Li/Ti order–disorder phase transition from a disordered cubic phase to an ordered cubic phase with increasing x values from 0.4 to 0.6. With increasing the A-site lithium content, the LCT ceramics exhibit improved dielectric permittivity ε_r (20.3–26.5), high $Q \times f$ value ($\geq$29 400 GHz) and a tailored temperature coefficient of resonant frequency τ_f from −40 to 10 ppm per °C. Optimized microwave dielectric properties were achieved for the composition with $x = 0.8$: $\varepsilon_r = 26.5$, $Q \times f \approx 29\,400$ GHz and $\tau_f \approx 10$ ppm per °C. A correlation between the cation distribution and microwave dielectric loss is discussed in detail.

1. Introduction

The development of miniature, lightweight and low cost microwave devices advanced dielectric materials with excellent dielectric properties (high quality factor ($Q \times f$), near-zero temperature coefficient of resonant frequency (τ_f) and moderate relative permittivity), and low bulk density.[1–3] Some commercial materials, such as Ba(Mg$_{1/3}$Ta$_{2/3}$)O$_3$ (BMT) and Ba(Zn$_{1/3}$Ta$_{2/3}$)O$_3$ (BZT),[4,5] possess a high quality factor ($Q \times f > 150\,000$), but high density and expensive cost restrict their applications in microwave devices. Other materials, such as (Zr$_{1-x}$Sn$_x$)TiO$_4$, BaTi$_4$O$_9$, Ba$_2$Ti$_9$O$_{20}$, are low cost materials,[6–8] however, a high sintering temperature together with a long annealing time is necessary to obtain densified ceramics. So, the search for new microwave dielectric materials with excellent properties, low cost and bulk density is in rapid progress owing to the drive for further system miniaturization.[9–11]

The spinel compounds have a general formulation of AB$_2$O$_4$ which crystallize in the cubic (isometric) crystal system. For this structure, the oxide anions are arranged in a cubic close-packed lattice and the cations A and B occupy some or all of the octahedral and tetrahedral sites in the lattice. A and B can be divalent, trivalent, or quadrivalent cations, including Mg, Zn, Fe, Mn, Al, Cr, Ti, and Si. Many spinel compounds have been widely investigated due to their outstanding magnetism (such as CoFe$_2$O$_4$, Ni$_{0.5}$Zn$_{0.5}$Fe$_2$O$_4$, ZnFe$_2$O$_4$, *etc.*)[12–14] and electrochemical properties (such as LiMn$_2$O$_4$, LiCo$_{0.5}$Mn$_{1.5}$O$_4$, Li$_4$Ti$_5$O$_{12}$, *etc.*).[15–17] Some compounds, such as ZnAl$_2$O$_4$, MgAl$_2$O$_4$, Mg$_2$TiO$_4$, *etc.* also exhibited perfect microwave dielectric performance,[18–20] however, high sintering temperature restricted their further applications. Recently, the microwave dielectric properties of Li-based spinel compounds Li$_2$MTi$_3$O$_8$ (M = Zn, Mg) have been reported by Sebastian *et al.*,[21] Zhou *et al.*[22] These materials not only showed excellent microwave properties, but also exhibited low sintering temperature, cheap raw materials cost and low bulk density. Antic *et al.*[23] reported that a complete range of spinel-like solid solutions Li$_{4x/3}$Co$_{2-2x}$Ti$_{1+2x/3}$O$_4$ ($0 \leq x \leq 1$) forms between Li$_4$Ti$_5$O$_{12}$ and Co$_2$TiO$_4$. Fang and Zhou[24,25] reported that two intermediate compounds LiCo$_{0.5}$Ti$_{1.5}$O$_4$ and Li$_{2/3}$CoTi$_{4/3}$O$_4$ exhibit good microwave dielectric properties, cheap cost and bulk density. However, the relationship between the structure and microwave dielectric properties of Li$_{4x/3}$Co$_{2-2x}$Ti$_{1+2x/3}$O$_4$ solid solutions has not been well-established. In this work, Li$_{4x/3}$Co$_{2-2x}$Ti$_{1+2x/3}$O$_4$ spinel series compounds were synthesized. The phase structure, cation distribution, order–disorder phase transition, microstructure and dielectric properties of these ceramics have also been investigated. Finally, correlations between the cation distribution and microwave dielectric loss are also addressed.

[a] School of Materials Science and Engineering, Guilin University of Technology, Guilin 541004, China. E-mail: zhouhuanfu@163.com

[b] School of Materials Science and Engineering, Nanyang Technological University, 50 Nanyang Avenue, Singapore, 639798, Singapore

[c] Electronic Materials Research Laboratory, Key Laboratory of the Ministry of Education, International Center for Dielectric Research, Xi'an Jiaotong University, Xi'an, 710049, Shaanxi, China

2.   Experimental procedure

Specimens of the $Li_{4x/3}Co_{2-2x}Ti_{1+2x/3}O_4$ (LCT, $0.2 \leq x \leq 0.8$) ceramics were prepared by the conventional mixed oxide route from the high-purity raw powders ($\geq$99%, Sinopharm Chemical Reagent Co. Ltd, Shanghai, China) of Li_2CO_3, Co_2O_3 and TiO_2. The stoichiometric proportions of the above raw materials were mixed in the high-purity alcohol medium using zirconia balls for 4 h. The mixtures were dried and calcined at 900 °C for 6 h in air. With subsequent ball-milling, the powders were mixed with 5 wt% polyvinyl alcohol and pressed in to pellets of 12 mm in diameter and 6–7 mm in height by uniaxial pressing under a pressure of 200 MPa. The pellets were heat-treated at 550 °C for 4 h to remove the organic binder and then sintered at 1050–1150 °C for 2 h with a heating rate of 5 °C min^{-1} in air.

The crystal structures of the specimens were analyzed by an X-ray diffractometer (CuK$_{\alpha 1}$, 1.54059 Å, Model X'Pert PRO, PANalytical, Almelo, Holland) with CuK$_\alpha$ radiation generated at 40 kV and 100 mA. Data of a quality suitable for Rietveld refinement were collected over a 3 h range of 10–120°. Structural analysis has been done using Rietveld refinement program Topas 4.1. As $0.2 \leq x \leq 0.4$, the parameters of Co_2TiO_4 were chose as a starting model. But when $0.6 \leq x \leq 0.8$, the starting model was $Li_2CoTi_3O_8$. It should be noted here that in order to avoid changing the multiplicity, the Wyckoff sites 8a and 16d with specific site symmetry in the structure with space group

$Fd\bar{3}m$ were fixed and not refined, neither for the sites 4b, 8c, 12d, and 24e sites with specific symmetry in the $P4_332$ space group. The bulk densities of the sintered samples were measured by the Archimedes method. After polishing and thermally etching, the samples were coated with gold and performed using a field emission scanning electron microscope (FESEM, JEOL JSM-7600F). Raman spectra were collected with a WITEC CRM200 Raman System (488 nm laser, 2.54 eV, WITec, Germany). Dielectric behaviors in microwave frequency were measured by the $TE_{01\delta}$ shielded cavity method using a Network Analyzer (Model N5230A, Agilent Co., Palo Alto, California) and a temperature chamber (Delta 9039, Delta Design, San Diego, California). The temperature coefficient of resonant frequency (τ_f) was calculated by the formula as following:

$$\tau_f = \frac{f_T - f_0}{f_0(T - T_0)}, \qquad (1)$$

where f_T, f_0 were the resonant frequencies at the measuring temperature T (85 °C) and T_0 (25 °C) respectively.

3.   Results

3.1   Cations distribution and crystal structure

The phase structure and cation distribution of $Li_{4x/3}Co_{2-2x}Ti_{1+2x/3}O_4$ (LCT) ceramics have been investigated by XRD refinement. Some of the intensities are not fit particularly well, this may mainly results from the deviation between the
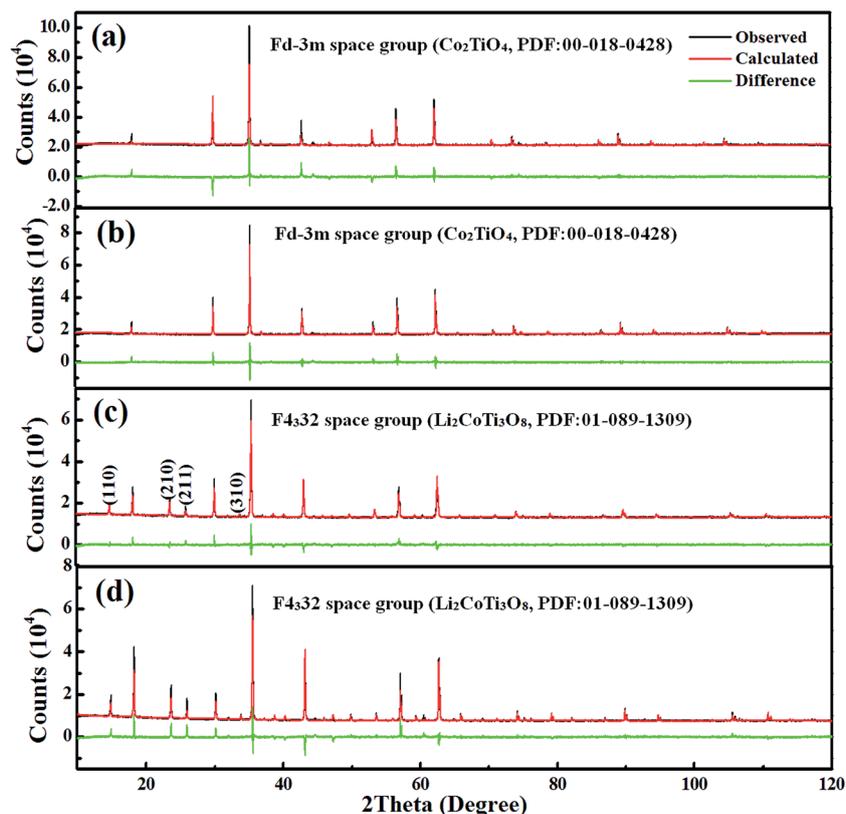

Fig. 1   XRD refinement of $Li_{4x/3}Co_{2-2x}Ti_{1+2x/3}O_4$ series: (a) $x = 0.2$ and (b) $x = 0.4$, were disordered phases, (c) $x = 0.6$ and (d) $x = 0.8$ were ordered phases. Indexed peaks are the superstructure of the ordered spinel phase.

nominal and refined composition, as it is indeed difficult to get an accurate position and ideal occupancy for Li atoms from XRD data due to its low scattering factor to the X-ray. As to a Rietveld refinement based on powder XRD data (not single crystal refinements), several R-indices, such as R_{wp}, R_p, R_{exp} et al., are used to check on the quality of the fit, and refinement R_{wp} is statistically the most meaningful indicator of the overall fit since the numerator is the residual that is minimized in the least squares procedure. Here, although the GOF ($= R_{wp}/R_{exp}$) value seems a bit high, the considerable low R_{wp} values for all these Rietveld refinements make the fitting results acceptable and reliable. Fig. 1 shows the XRD patterns of all the products in $Li_{4x/3}Co_{2-2x}Ti_{1+2x/3}O_4$ series. It can be seen that as the x values increased from 0.4 to 0.6, additional superstructural peaks appeared in the XRD patterns. All these reflections were indexed satisfactorily on the basis of a cubic unit cell [Co_2TiO_4 (PDF: 00-018-0428)] (Fig. 1(b)). The appearance of extra peaks agreed well with the previous report.[22] In Leonidov's work,[26] the reflections viz. (110), (210), (211), (221), and (310) which belong to superstructural peaks, appeared in XRD pattern due to the ordering of Li ion and Ti ion at octahedral site. Therefore, the sample, $x = 0.6$ exhibits cation ordering (Li : Ti = 1 : 3) on the octahedral sites, resulting in a superstructure that could be refined in the $P4_332$ space group [$Li_2CoTi_3O_8$ (PDF: 01-0891309)]. The crystallographic data for $Li_{4x/3}Co_{2-2x}Ti_{1+2x/3}O_4$ compounds obtained by the Rietveld refinement are listed in Table 1. All the Bragg reflections were indexed on the basis of a cubic symmetry. With increasing the x values, the LCT samples undergo a disorder–order phase transition from the space group $Fd\bar{3}m$ to $P4_332$. Antic et al.[23] reported that $Li_{4x/3}Co_{2-2x}Ti_{1+2x/3}O_4$ ($0.5 \leq x \leq 0.875$) exhibited 3 : 1 cation ordering with an ideal composition $x = 0.75$, i.e., $Li_2CoTi_3O_8$. In our work, as the x value exceeds 0.6, the 1 : 3 ordered structure at the octahedral site is represented by lithium (4b) and titanium (12d), although the titanium sublattice contains some Co. The crystal structures of $Li_{4x/3}Co_{2-2x}Ti_{1+2x/3}O_4$ series for $x = 0.4$ and $x = 0.6$, obtained from the Rietveld refinement data, are demonstrated in Fig. 2. It can be seen that as $x = 0.4$, the crystal

Table 1 Crystal structure data and cation composition of $Li_{4x/3}Co_{2-2x}Ti_{1+2x/3}O_4$ series

| Atom	Site	x/a	y/b	z/c	O_{cc}	B_{eq}
$x = 0.2$, $(Li_{0.12}Co_{0.87}Ti_{0.01})(Li_{0.15}Co_{0.73}Ti_{1.12})O_4$, space group $Fd\bar{3}m$, disordered phase						
Co	8a	0	0	0	0.8738(3)	0.6727(1)
Li	8a	0	0	0	0.1162(3)	0.6727(1)
Ti	8a	0	0	0	0.01(1)	0.6727(1)
Co	16d	5/8	5/8	5/8	0.3832(2)	0.6727(1)
Li	16d	5/8	5/8	5/8	0.1508(3)	0.6727(1)
Ti	16d	5/8	5/8	5/8	1/2	0.6727(1)
O	32e	0.3802(2)	0.3802(2)	0.3802(2)	1	1
$R_{exp} = 0.92$, $R_{wp} = 4.17$, $R_p = 1.74$, GOF = 4.52, DW = 0.39, $a = 8.4308(3)$						
$x = 0.4$, $(Li_{0.16}Co_{0.83}Ti_{0.01})(Li_{0.37}Co_{0.37}Ti_{1.26})O_4$, space group $Fd\bar{3}m$, disordered phase						
Co	8a	0	0	0	0.8299(1)	0.759(4)
Li	8a	0	0	0	0.1601(5)	0.759(4)
Ti	8a	0	0	0	0.01(1)	0.759(4)
Co	16d	5/8	5/8	5/8	1/2	0.759(4)
Ti	16d	5/8	5/8	5/8	0.3663(3)	0.759(4)
Li	16d	5/8	5/8	5/8	0.1337(2)	0.759(4)
O	32e	0.3802(2)	0.3802(2)	0.3802(2)	1	1
$R_{exp} = 0.75$, $R_{wp} = 1.62$, $R_p = 0.83$, GOF = 2.15, DW = 0.95, $a = 8.4137(4)$						
$x = 0.6$, $(Li_{0.31}Co_{0.69})(Li_{0.49}Co_{0.11}Ti_{1.4})O_4$, space group $P4_332$, ordered phase						
Li	4b	5/8	5/8	5/8	0.9797(6)	0.8899(2)
Co	8c	0	0	0	0.6898(1)	0.8899(2)
Li	8c	0	0	0	0.3102(5)	0.8899(2)
Ti	12d	1/8	3/8	−1/8	0.952(3)	0.8899(2)
Co	12d	1/8	3/8	−1/8	0.048(2)	0.8899(2)
O	24e	1/8	1/8	3/8	1	1
O	8c	3/8	3/8	3/8	1	1
$R_{exp} = 0.85$, $R_{wp} = 1.66$, $R_p = 0.98$, GOF = 1.95, DW = 0.51, $a = 8.3898(2)$						
$x = 0.8$, $(Li_{0.6}Co_{0.4})(Li_{0.47}Ti_{1.53})O_4$, space group $P4_332$, ordered phase						
Li	4b	5/8	5/8	5/8	0.8(1)	1.239(6)
Co	8c	0	0	0	0.4(1)	1.239(6)
Li	8c	0	0	0	0.6(1)	1.239(6)
Ti	12d	1/8	3/8	−1/8	1	1.239(6)
O	24e	1/8	1/8	3/8	1	1
O	8c	3/8	3/8	3/8	1	1
$R_{exp} = 1.09$, $R_{wp} = 3.86$, $R_p = 2.01$, GOF = 3.55, DW = 0.38, $a = 8.3748(3)$						
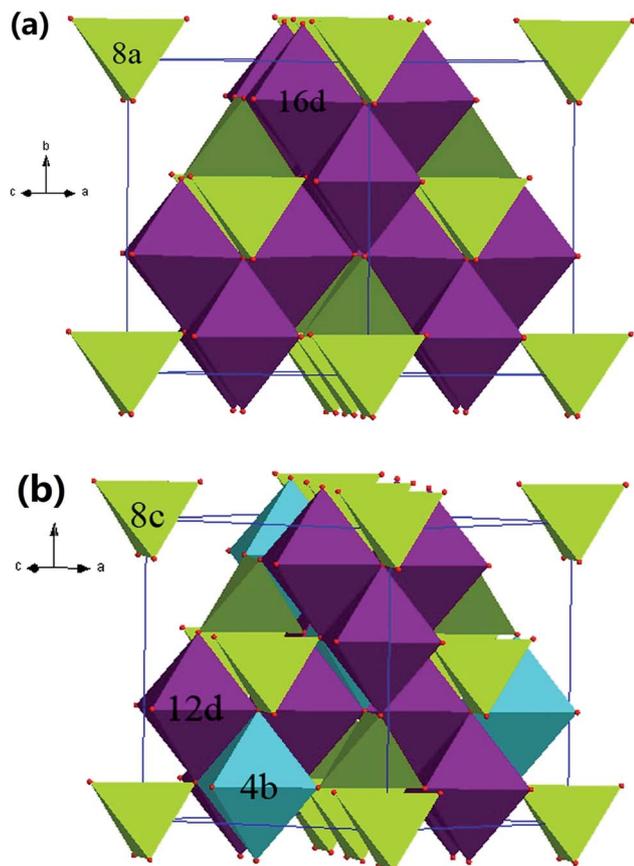
Fig. 2 (a) Crystal structure of $Li_{4x/3}Co_{2-2x}Ti_{1+2x/3}O_4$ series for $x = 0.4$, where 8a is the $(Li_{0.16}Co_{0.83}Ti_{0.01})O_4$, 16d is the $(Li_{0.37}Co_{0.37}Ti_{1.26})O_6$; (b) $x = 0.6$, where 8c is the $(Li_{0.31}Co_{0.69})O_4$, 12d and 4b are the $(Li_{0.49}Co_{0.11}Ti_{1.4})O_6$.

Fig. 3 (a) Raman spectra of the $Li_{4x/3}Co_{2-2x}Ti_{1+2x/3}O_4$ series, (b) high-resolution Roman spectra of $Li_{4x/3}Co_{2-2x}Ti_{1+2x/3}O_4$ ($x = 0.6$ and 0.8) ceramics in the range of 200–600 cm^{-1}.

was a disordered phase in which cations occupied 8a and 16d Wyckoff's positions. When the $x = 0.6$, the crystal became ordered phase and the cations occupied 8c, 4b, and 12d Wyckoff's positions. The Li at 4b position and Ti at 12d position formed a 1 : 3 order in the octahedral.

3.2 Raman analysis

Fig. 3 illustrates the Raman spectroscopy of $Li_{4x/3}Co_{2-2x}Ti_{1+2x/3}O_4$ ceramics. Comparing with the powder XRD techniques, Raman spectroscopy reflects a short-range environment of the oxygen coordination around the cations in oxides or compounds. The positions and relative intensities of the Raman modes are sensitive to coordination geometry, oxidation states, and Jahn–Teller distortions.[27,28] For the disordered spinel-type compounds ($Fd\bar{3}m$ space group), five optic modes are Raman active: 32e (O): $A_{1g} + E_g + 2F_{2g}$, 8a (cations): $1F_{2g}$. Ordering of the cations on octahedral sites will reduce the crystal symmetry from $Fd\bar{3}m$ to $P4_332$. As a result, the number of Raman active modes will increase dramatically ($5A1 + 12E + 17F2$). Accordingly, atoms in all Wyckoff's position are Raman active: 8c: ($1A1 + 2E + 3F2$), 4b: ($1E + 1F2$), 24e: ($3A1 + 6E + 9F2$), 12d: ($1A1 + 3E + 4F2$). Therefore, the phase transition in $Li_{4x/3}Co_{2-2x}Ti_{1+2x/3}O_4$ can be easily recognized from Raman spectra. As the $x \leq 0.4$, three weak and
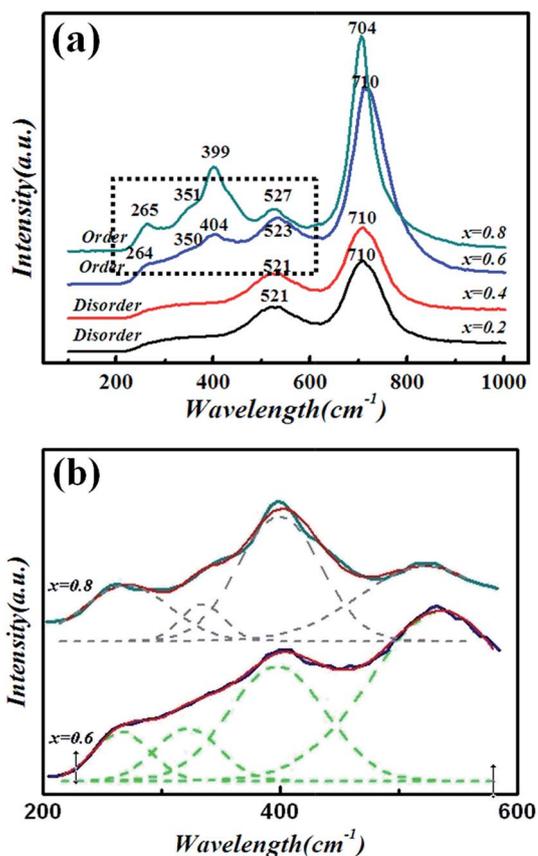
broad bands around 350, 530, and 700 cm^{-1} could be observed. When the x value reaches 0.6, the Raman spectrum shows stronger and intense Raman bands at 710, 526, 404, 356 and 264 cm^{-1}, which is probably the consequence of the 1 : 3 ordering of lithium and titanium in the octahedral sublattice. In Bouchard's work,[29] Raman spectra of $LiCo_{0.5}Ti_{1.5}O_4$ ($x = 0.75$) ordered spinel compound exhibit intense, broad bands at 700 and 400 cm^{-1} and minor bands at 528, 349 and 262 cm^{-1}, which agree well with the results of the ordered samples for $x = 0.6$ and 0.8. The Raman active modes were assigned and the results were listed in Table 2.
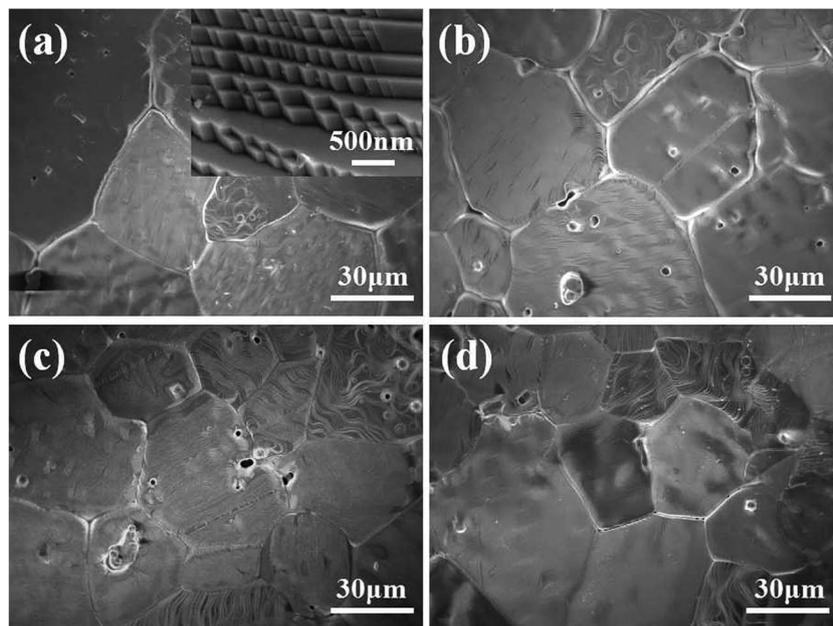
Table 2 Raman active modes of $Li_{4x/3}Co_{2-2x}Ti_{1+2x/3}O_4$ compounds

$Li_{4x/3}Co_{2-2x}Ti_{1+2x/3}O_4$	Disordered cubic phase		Ordered cubic phase	
Raman mode (cm^{-1})	$x = 0.2$	$x = 0.4$	$x = 0.6$	$x = 0.8$
A_{1g}	710	710	710	704
F_{2g}	521	521	523	527
E_g	—	—	404	399
F_{2g}	346	348	350	351
F_{2g}	—	—	264	265

Fig. 4 SEM of $Li_{4x/3}Co_{2-2x}Ti_{1+2x/3}O_4$ ceramics: (a) $x = 0.2$, (b) $x = 0.4$, (c) $x = 0.6$ and (d) $x = 0.8$. Inset shows the enlarged SEM of (a).

3.3 Microstructure analysis

The surface images of the $Li_{4x/3}Co_{2-2x}Ti_{1+2x/3}O_4$ ceramics have been examined by SEM and showed in Fig. 4. All samples exhibited uniform grain growth and few pores can be observed. The average grain size is about 50 μm, with reasonably good close packing of grains. Through enlarging some part of the grains, the step growth mechanism will be revealed [as seen in the inset of Fig. 4(a)].

3.4 Microwave dielectric properties

The microwave dielectric properties of $Li_{4x/3}Co_{2-2x}Ti_{1+2x/3}O_4$ series compounds sintered at their optimized temperatures are listed in Table 3. With increasing x values, the optimized sintering temperature of solution decreased from 1125 to 1075 °C. The ceramics obtained a high relative density (over 95%). The permittivity was corrected by the Rushman–Strivens formula:[30] $\varepsilon_{r.c.} = \varepsilon_{r.m.} \times (2 + P)/2(1 - P)$, where P is the porosity, $\varepsilon_{r.c.}$ and $\varepsilon_{r.m.}$ are the corrected permittivity and measured permittivity, respectively. The measured permittivity increased from 20.3 to 26.5, τ_f value improved from −40.1 to 10 ppm per °C and $Q \times f$ value deceased from 67 400 to 29 400 GHz. In a word, the ceramic for $x = 0.8$ exhibits good microwave dielectric properties with: $\varepsilon_{r.m.} = 26.5$, $Q \times f = 29\,400$ GHz, and $\tau_f = 10$ ppm per °C (Table 3).

3.5 Infrared reflectivity

Fig. 5 presents the IR reflectivity spectra of $Li_{4x/3}Co_{2-2x}Ti_{1+2x/3}O_4$ ($x = 0.2$ and 0.8) ceramics ranging from 50 to 1000 cm^{-1}. It is seen that the infrared spectra were fitted by 7 resonant modes corresponding with the infrared reflectivity peaks and the reflectivity intensities of bands below 300 cm^{-1} become weaker for $x = 0.2$. For $x = 0.8$, the infrared spectra were fitted by 13 resonant modes and the bands above 700 cm^{-1} become weaker.
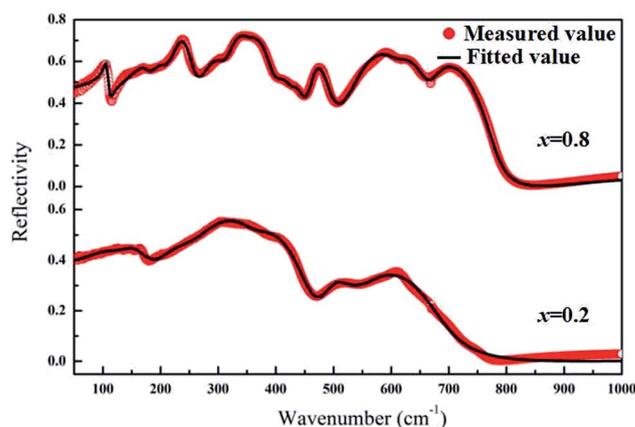
Table 3 The relative permittivity, $Q \times f$ and τ_f values of $Li_{4x/3}Co_{2-2x}Ti_{1+2x/3}O_4$ series sintered their optimized temperature

$Li_{4x/3}Co_{2-2x}Ti_{1+2x/3}O_4$	$x = 0.2$	$x = 0.4$	$x = 0.6$	$x = 0.8$
Sintering temperature (°C)	1125	1100	1075	1075
Relative density (%)	96	95.4	95.8	95.7
$\varepsilon_{r.m.}$	20.3	20.9	24.8	26.5
$\varepsilon_{r.c.}$	21.6	22.4	26.4	28.3
$Q \times f$ (GHz)	67 400	65 300	43 300	29 400
f (GHz)	7.81	7.32	7.08	6.27
τ_f (ppm per °C)	−40.1	−32	−15.8	10

Fig. 5 IR reflectivity spectra of $Li_{4x/3}Co_{2-2x}Ti_{1+2x/3}O_4$ ($x = 0.2$ and 0.8) ceramics ranging from 50 to 1000 cm^{-1}.

There spectra have been analyzed by using the classical harmonic oscillator model based on the standard Lorentzian formula [eqn (2)] and the Fresnel formula [eqn (3)]:

$$\varepsilon^*(\omega) = \varepsilon_\infty + \sum_{j=1}^{n} \frac{\omega_{pj}^2}{\omega_{oj}^2 - \omega^2 - i\gamma_j\omega}, \tag{2}$$

$$R(\omega) = \left| \frac{1 - \sqrt{\varepsilon^*(\omega)}}{1 + \sqrt{\varepsilon^*(\omega)}} \right|^2, \tag{3}$$

where $\varepsilon^*(\omega)$ is complex dielectric function. ε_∞ is the dielectric constant caused by the electronic polarization at high frequencies. ω_{pj}, ω_{oj} and γ_j are the plasma frequency, the transverse frequency, and damping factor of the j-th Lorentz oscillator, respectively. n is the number of transverse phonon modes. $R(\omega)$ is the IR reflectivity.

Fig. 6 shows the calculated permittivity $\varepsilon'(\omega)$ and loss $\varepsilon''(\omega)$ obtained from the fits of the infrared reflectivity together with the experimental microwave data. It is seen that the calculated permittivities are a little smaller than the measured ones in the microwave range. Meanwhile, the calculated and measured dielectric losses have the same order of magnitudes. Therefore, it can be concluded that the microwave dielectric properties of ceramics are mainly caused by the polar optical phonons.
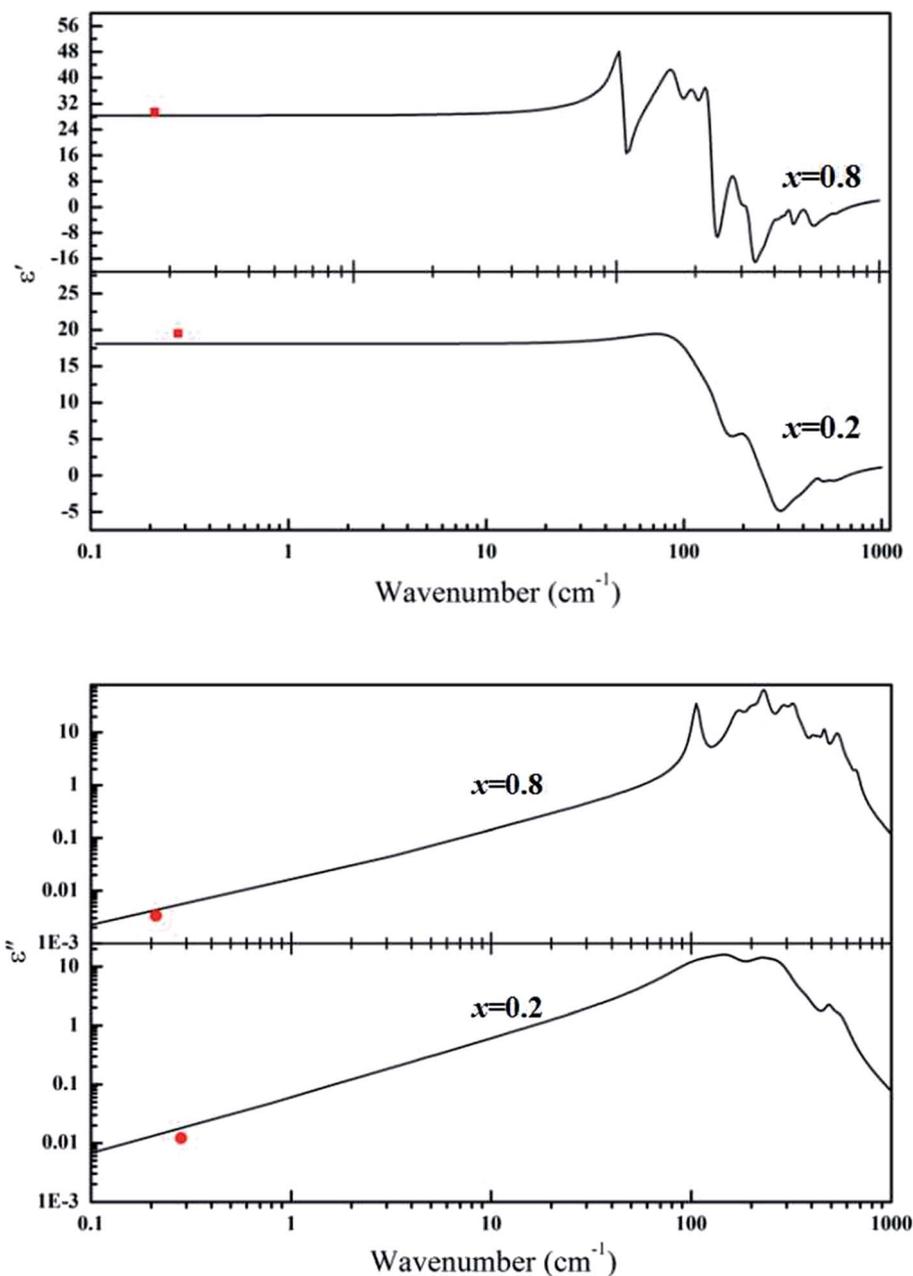

Fig. 6 The calculated permittivity $\varepsilon'(\omega)$ and loss $\varepsilon''(\omega)$ obtained from the fits of the infrared reflectivity together with the experimental microwave data (the red dots represent the experimental values that measured by using TE$_{01\delta}$ method).
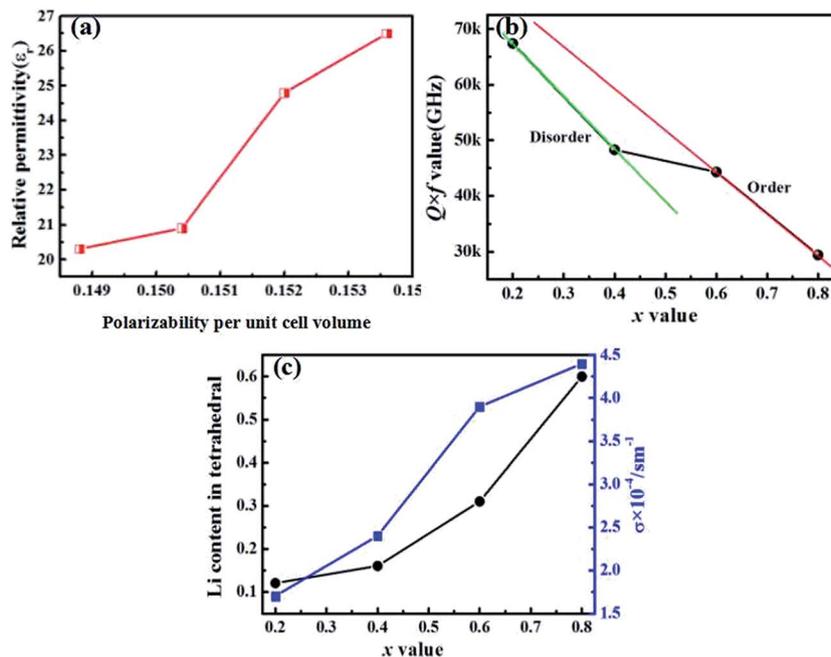
Fig. 7 (a) Relative permittivity *vs.* polarizability per unit volume, (b) $Q \times f$ as a function of x value, and (c) σ and Li occupation in tetrahedral as a function of x value.

4. Discussion

For the Li-based spinel compounds, the cations distribution in the octahedral and tetrahedral plays an important role on tailoring the properties. Fig. 7(a) illustrates the relationship between the ionic polarizability per unit cell volume (α_v) and relative permittivity. The variation of relative permittivity through the compositional evolution is dependent on the ionic polarizability per unit cell volume (α_v).[31] The α_v increased from 0.1488 to 0.1536 with increasing x values, which results the increase of relative permittivity. The τ_f values increased from -40 to 10 ppm per °C with increasing x values. The behavior of the change of τ_f in this solid solution is similar to K_2NiF_4 type ceramic $SrLaAlO_4$–Sr_2TiO_4 system.[31] The origin of τ_f is related to linear expansion coefficient α_L and dielectric constant variation with temperature (τ_ε). Mathematically, the relationship is:

$$\tau_f = \frac{1}{f}\frac{\partial f}{\partial T} = -\left(\alpha_L + \frac{1}{2}\tau_\varepsilon\right), \qquad (4)$$

where τ_ε is the temperature coefficient of the permittivity and α_L is the linear thermal expansion coefficient of the dielectric material which is usually positive. For most of the electronic ceramic materials, α_L is about $+10$ ppm per °C, indicating the significant influence of τ_ε on τ_f. ε_r increases with increasing x value, the polarizability per unit cell volume increases. Meanwhile, the long range coupling of Ti^{4+} is improved through decreasing the Co^{2+} concentration. These effects drive τ_ε more negatively, which in turn makes τ_f increase toward zero and positive further.

The $Q \times f$ values of $Li_{4x/3}Co_{2-2x}Ti_{1+2x/3}O_4$ series ceramics decreased with increasing the x values [as shown in Fig. 7(b)]. The microwave dielectric losses included intrinsic loss which were mainly contributed by the lattice vibrational modes and extrinsic loss caused by densification/porosity, grain sizes, secondary phases and oxygen vacancies. For the $Li_{4x/3}Co_{2-2x}Ti_{1+2x/3}O_4$ series ceramics, the changing $Q \times f$ values were related to the lattice vibrational loss and conductivity loss. From the XRD analysis, as the x values increase from 0.4 to 0.6, the crystal system changed from a disordered to ordered phase, indicating the increase of $Q \times f$ values. For the same composition for LCT compounds, an ordered phase exhibits a higher $Q \times f$ value than the disordered phase. The similar phenomenon was observed in $Ba_3MM'_2O_9$ (M = Mg, Ni, Zn; M' = Nb, Ta) perovskite compounds.[5,32] Fig. 7(c) illustrated the relationship between the conductivity, lithium content in tetrahedral and x values. It can be seen that the conductivity and lithium content in tetrahedral increased with increasing x values. Higher lithium content in tetrahedral induced a higher conductivity loss. As a result, the $Q \times f$ values decreased. Besides, the atoms must overcome much force because of the shrinkage of the cell. These two factors induced the higher dielectric loss for the $Li_{4x/3}Co_{2-2x}Ti_{1+2x/3}O_4$ series compounds. $Li_{4x/3}Co_{2-2x}Ti_{1+2x/3}O_4$ exhibited good microwave dielectric performances, but high sintering temperature (1075–1125 °C) limit their further industrial applications, we will try to reduce the sintering temperature of $Li_{4x/3}Co_{2-2x}Ti_{1+2x/3}O_4$ ceramics in the next work.

5. Conclusions

In this paper, $Li_{4x/3}Co_{2-2x}Ti_{1+2x/3}O_4$ spinel series compounds were synthesized. The phase structure, cation distribution, order–disorder phase transition, microstructure and dielectric properties of these ceramics have also been investigated.

Structural analysis showed that the $Li_{4x/3}Co_{2-2x}Ti_{1+2x/3}O_4$ series undergo a discontinuous phase transition from a disordered cubic phase to an ordered cubic phase with the changing x value. $Li_{4x/3}Co_{2-2x}Ti_{1+2x/3}O_4$ ceramics exhibit relatively high dielectric permittivity ε_r of 20.3–26.5, modest $Q \times f$ values of 29 400–67 400 GHz and temperature coefficient of resonant frequency τ_f from −40 ppm per °C to 10 ppm per °C. Finally, correlations between the cation distribution and microwave dielectric loss are also addressed.

Conflicts of interest

There are no conflicts to declare.

Acknowledgements

References

1 D. Zhou, D. Guo, W. B. Li, L. X. Pang, X. Yao, D. W. Wang and I. M. Reaney, *J. Mater. Chem. C*, 2016, **4**, 5357.

2 B. Liu, L. Li, X. Q. Liu and X. M. Chen, *J. Mater. Chem. C*, 2016, **4**, 4684.

3 J. Guo, C. A. Randall, G. Q. Zhang, D. Zhou, Y. Y. Chen and H. Wang, *J. Mater. Chem. C*, 2014, **2**, 7364.

4 K. P. Surendran, M. T. Sebastian, P. Mohanan, R. L. Moreira and A. Dias, *Chem. Mater.*, 2005, **17**, 142.

5 M. W. Lufaso, *Chem. Mater.*, 2004, **16**, 2148.

6 K. Wakino, K. Minai and H. Tamura, *J. Am. Ceram. Soc.*, 1984, **67**, 278.

7 S. G. Mhaisalker, D. W. Ready and S. A. Akbar, *J. Am. Ceram. Soc.*, 1991, **74**, 1894.

8 S. F. Wang, Y. F. Hsu, T. H. Weng, C. C. Chiang, J. P. Chu and C. Y. Huang, *J. Mater. Res.*, 2003, **18**, 1179.

9 D. Zhou, L. X. Pang, J. Guo, H. Wang, X. Yao and C. Randall, *Inorg. Chem.*, 2011, **50**, 12733.

10 J. J. Bian and J. Y. Wu, *J. Am. Ceram. Soc.*, 2012, **95**, 318.

11 C. L. Huang, Y. W. Tseng and J. Y. Chen, *J. Eur. Ceram. Soc.*, 2012, **32**, 3287.

12 H. Zheng, J. Wang, S. E. Lofland, Z. Ma, L. Mohaddes-Ardabili, T. Zhao, L. Salamanca-Riba, S. R. Shinde, S. B. Ogale, F. Bai, D. Viehland, Y. Jia, D. G. Schlom, M. Wuttig, A. Roytburd and R. Ramesh, *Science*, 2004, **303**, 661.

13 I. Ismayadi, M. Hashim, A. M. Khamirul and R. Alias, *Am. J. Appl. Sci.*, 2009, **6**, 1548.

14 C. Yao, Q. Zeng, G. F. Goya, T. Torres, J. Liu, H. Wu, M. Ge, Y. Zeng, Y. Wang and J. Z. Jiang, *J. Phys. Chem. C*, 2007, **111**, 12274.

15 S. H. Guo, S. C. Zhang, X. M. He, W. H. Pu, C. Y. Jiang and C. R. Wan, *J. Electrochem. Soc.*, 2008, **155**, A760.

16 A. R. West, H. Kawai, H. Kageyama, M. Tabuchi, M. Nagata and H. Tukamoto, *J. Mater. Chem.*, 2001, **11**, 1662.

17 G. J. Wang, J. Gao, L. J. Fu, N. H. Zhao, Y. P. Wu and T. Takamura, *J. Power Sources*, 2007, **174**, 1109.

18 W. Lei, W. Z. Lu, J. H. Zhu and X. H. Wang, *Mater. Lett.*, 2007, **61**, 4066.

19 K. P. Surendran, P. V. Bijumon, P. Mohanan and M. T. Sebastian, *Appl. Phys. A*, 2005, **81**, 823.

20 C. L. Huang and J. Y. Chen, *J. Am. Ceram. Soc.*, 2009, **92**, 675.

21 S. George and M. T. Sebastian, *J. Am. Ceram. Soc.*, 2010, **93**, 2164.

22 H. F. Zhou, X. L. Chen, L. Fang and H. Wang, *J. Mater. Res.*, 2010, **25**, 1235.

23 B. Antic, G. F. Goya, V. Kusigerski, N. Jovic, M. Mitric and H. R. Rechenberg, *J. Phys.: Condens. Matter*, 2004, **16**, 651.

24 L. Fang, D. Chu, H. Zhou, X. Chen and Z. Yang, *J. Alloys Compd.*, 2011, **509**, 1880.

25 H. F. Zhou, X. B. Liu, X. L. Chen and L. Fang, *Mater. Res. Bull.*, 2012, **47**, 1278.

26 I. Leonidov, N. Leonidova, R. F. Samigullina and V. Patrakeev, *J. Struct. Chem.*, 2004, **45**, 262.

27 C. M. Julien, F. Gendron, A. Amdouni and M. Massot, *Mater. Sci. Eng., B.*, 2006, **130**, 41.

28 N. Jovic, M. Vucinic-Vasic, A. Kremenovic, B. Antic, C. Jovalekic, P. Vulic, V. Kahlenberg and R. Kaindl, *Mater. Chem. Phys.*, 2009, **116**, 542.

29 M. Bouchard and A. Gambardella, *J. Raman Spectrosc.*, 2010, **41**, 1477.

30 D. F. Rushman and M. A. Strivens, *Proc. Phys. Soc.*, 1947, **59**, 1011.

31 M. M. Mao, X. M. Chen and X. Q. Liu, *J. Am. Ceram. Soc.*, 2011, **94**, 3948.

32 M. Bieringer, S. M. Moussa, L. D. Noailles, A. Burrows, C. J. Kiely, M. J. Rosseinsky and R. M. Ibberson, *Chem. Mater.*, 2003, **15**, 586.